Mathematical Biosciences and Engineering

MBE, 21 (2): 2879–2900.
DOI:10.3934/mbe.2024128
Received: 14 November 2023
Revised: 14 January 2024
Accepted: 18 January 2024
Published: 25 January 2024

http://www.aimspress.com/journal/MBE

Research article

Torque control strategy of electric racing car based on acceleration intention recognition

Anlu Yuan*, Tieyi Zhang, Lingcong Xiong, and Zhipeng Zhang

School of Mechanical Engineering, Guangxi University, Nanning 530004, China

* **Correspondence:** Email: 1948744749@qq.com.

Abstract: A torque control strategy based on acceleration intention recognition is proposed to address the issue of insufficient power performance in linear torque control strategies for electric racing cars, aiming to better reflect the acceleration intention of racing drivers. First, the support vector machine optimized by the sparrow search algorithm is used to recognize the acceleration intention, and the running mode of the racing car is divided into two types: Starting mode and driving mode. In driving mode, based on the recognition results of acceleration intention, fuzzy control is used for torque compensation. Based on the results of simulation and hardware in the loop testing, we can conclude that the support vector machine model optimized using the sparrow search algorithm can efficiently identify the acceleration intention of racing drivers. Furthermore, the torque control strategy can compensate for positive and negative torque based on the results of intention recognition, significantly improving the power performance of the racing car.

Keywords: accelerated intention recognition; compensation of torque; fuzzy control; support vector machine; SSA; torque control

1. Introduction

1.1. Background and present situation

Because of their significant contributions in reducing the world's energy scarcity, environmental deterioration, and greenhouse impact, electric vehicles are growing quickly, and related technologies are now the subject of scholarly study. Initiated in 2013, the Formula Student Electric Competition of

China (FSEC) aims to advance the growth of the electric vehicle industry and pique the interest of Chinese university students in innovative electric vehicle technological advances. The participating teams not only showcase their engineering practice abilities by designing, testing, and building electric racing cars on their own, but they also encourage the adoption of electric vehicle technology among university students. In addition to providing a forum for fostering young people's interest in sustainable transportation and renewable energy, FSEC establishes the groundwork for the advancement of electric car technology. The drive torque control technique is the foundation of vehicle control technology, even though it plays a significant role in the realm of electric vehicles. This method is responsible for figuring out the powertrain's output, which directly affects the vehicle's dynamics, economy, and comfort. However, many studies on electric racing cars often overlook the torque control during the initial acceleration phase. Additionally, they neglect scenarios where there is a negative rate of change in the accelerator pedal position. This oversight contributes to the subpar performance of FSEC electric racing cars in power test events, such as the 75-meter straight-line acceleration test.

1.2. Status of research on driving intention recognition

Research [1–4] centered on driving intention recognition equips vehicle systems with a deeper understanding of a driver's intentions. This comprehensive insight enhances the efficacy of driver assistance systems, bolstering safety and efficiency in intelligent transport systems. Given the potential hazards stemming from unclear driving intentions, particularly in the context of assisted driving systems (ADAS), predicting these intentions becomes paramount. The Long Short-Term Memory (LSTM) predictive model, as referenced in literature [5–9], adeptly discerns the driving intentions of electric car drivers under real-world conditions, thereby fortifying safety measures. References [10–14] leveraged neural networks for intent detection, refining their models through diverse operational scenarios. This article juxtaposes the Support Vector Machine (SVM) model—known for its superior performance and robust generalization capabilities in limited sample scenarios—against other pattern recognition techniques. In scenarios with a mix of autonomous and human-driven vehicles, accurately predicting the intentions of nearby human-driven vehicles becomes indispensable for the safe navigation of autonomous ones. Literature [15,16] introduces a driving intention prediction approach grounded in a Hidden Markov Model and cGAN-LSTM model. Simulation results validate that this method augments electric vehicle performance. Further, research [17,18] delves into the intricacies of electric racing car dynamics, shedding light on cutting-edge driving control strategies rooted in pattern recognition. This exploration also delves into the coordinated control of hybrid electric vehicles, emphasizing the challenges and solutions related to driving mode transitions. Such insights are invaluable for enhancing the efficiency and integration of diverse power sources within vehicle systems.

While various methodologies discern driving intentions, the SVM model stands out, particularly when dealing with limited training samples. Its generalization prowess surpasses that of methodologies like Hidden Markov Models and Neural Network Models. Consequently, this paper employs an SVM model, augmented by the sparrow search algorithm, to discern racing driver acceleration intentions.

1.3. Research Status of Torque Control Strategies for Electric Vehicles

The control strategy for torque distribution stands as a pivotal aspect of overall vehicle management in electric racing cars. Reference [19] delved into torque control strategies for new energy hybrid vehicles, emphasizing the application of fuzzy control methods for torque compensation. This involves discerning driver intentions and refining techniques to enhance energy efficiency, elevate vehicle performance, and cater to diverse driving scenarios. The strategies introduced facilitate a seamless power upshift, ensuring consistent traction torque and bolstering vehicle performance. Reference [20] outlines a torque compensation approach designed to minimize ripples during shifts in electric vehicles, leveraging this compensation method to optimize output torque. Reference [21] introduces a hierarchical control structure-driven strategy. This method fine-tunes the motor's reference torque allocation, synchronizing with the instantaneous power optimization of the economic module. The torque compensation from the dynamic module employs fuzzy control, boosting performance under intense dynamic conditions. Similarly, reference [22] proposed a torque control method for parallel hybrid electric vehicles, yielding improvements in both power output and efficiency. References [23–26] converge on torque compensation control strategies, emphasizing voltage increments to offset torque reduction arising from motor stator winding resistance. This ensures a smooth start and acceleration for the motor. In the realm of electric vehicles, torque distribution strategies are paramount for enhancing dynamics, curtailing energy consumption, and upholding safety standards. Literature [27–31] introduces energy-efficient torque distribution tactics centered on stability and conservation. These tactics bolster vehicle efficiency and amplify braking energy recovery. They offer robust theoretical and empirical insights endorsing torque distribution optimization in electric vehicles. Conversely, references [32–35] factor in motor torque attributes and road adhesion constraints. They devise torque distribution schemes through rigorous modeling and simulation, encompassing predictive control mechanisms, distribution based on the Karush-Kuhn-Tucker (KKT) condition, and optimization strategies for various torque distribution paradigms. These contributions underscore the synergistic blend of theory and practice in electric vehicle torque distribution. In academic works [36–41], torque compensation and driver intent recognition are integrated via adept fuzzy control techniques. This not only refines torque response through fuzzy logic but also accommodates variations in driver behavior, forging a cohesive bridge between driving intentions and torque application.

Contemporary studies on torque control for electric vehicles predominantly emphasize enhancing stability and curbing energy consumption. Notably, considerable advancements have emerged in hub motor applications and multi-motor system investigations. Nonetheless, we take a pioneering approach by centering on torque compensation strategies tailored for mitigating energy loss and performance decline in defined operational scenarios. By implementing a compensation mechanism, our objective is to tackle potential energy inefficiencies and performance setbacks in electric vehicles under specific conditions. This innovative trajectory seeks to introduce fresh perspectives and methodologies to torque distribution strategies within the electric vehicle domain, ultimately elevating the vehicle's overall energy efficiency and performance.

1.4. Research contents

To precisely align the electric racing car's actions with the driver's intentions, we employ a

Support Vector Machine (SVM) to discern acceleration intent. The SVM's penalty parameter 'c' and kernel function parameter 'g' are fine-tuned using the Sparrow Search Algorithm (SSA). Concurrently, we categorize the driving modes of the electric racing car into initiation and continuous driving modes, applying distinct torque control strategies to each. Comprehensive vehicle modeling, simulation analyses, and real-world hardware testing validate this approach. Detailed scrutiny and comparison of simulation and hardware test outcomes ascertain whether the driving intention-based control strategy enhances the racing car's power performance effectively.

2. Torque control strategy based on acceleration intention recognition

2.1. Accelerate intention recognition

2.1.1. Support Vector Machine Accelerated Intent Recognition

The driver's driving intention is multifaceted and includes acceleration, braking, and lane-changing intentions. This study focuses primarily on the driver's acceleration intention. The driver's intention to accelerate is directly reflected in the opening and rate of change of the accelerator pedal, which is identified by SVM as a feature parameter.

Assuming a feature space of R^n, $x_i \in R^n, i = 1,2,\cdots,n$, represents the i-th n-dimensional input vector, $y_i \in \{-1,\ 1\}$ is the input samples category, and when the samples to be classified $(x_i,\ y_i)$, $i = 1,2,\cdots,m$, are linearly separable, there exists a classification hyperplane to correctly separate the two types of samples.

To make a classification sample linearly separable when it is nonlinearly separable in the original feature space, a specific transformation must be applied to map the original nonlinearly separable space to the new feature space. This change adds a processing kernel function. The kernel function chooses the Gaussian kernel function as the feature transformation function of SVM and translates low-dimensional data to high-dimensional space, replacing the inner product of the original feature space for function computation.

$$K(X_i \cdot X_j) = e^{\left(-\frac{\|x_i - x_j\|^2}{2g^2}\right)} \tag{1}$$

Data samples must first be trained to use SVM models to detect racing drivers' intentions to accelerate. We employ the acceleration intention as the classification label and the accelerator pedal opening and its rate of change as the SVM feature recognition parameters. The three categories that make up the acceleration intention, denoted by the numerals 1, 2, and 3, describe the race driver's need for gradual acceleration, general acceleration, and emergency acceleration, respectively.

A total of 200 sets of driving sample data were simulated under various cycle conditions, including NEDC, FTP75, and racing durability testing, using the electric racing model integrated within the AVL-cruise program. Following normalization, 60 sets of driving sample data were used as test sample data, and 140 sets of driving sample data were utilized as training sample data. Some sample data are displayed in Table 1.

Set the RBF kernel kernel function type, the kernel function parameter g to 0.5, and the penalty

parameter c to 1. Figure 1 displays the SVM classification outcomes attained through running.

SVM can recognize the intention of racing drivers to accelerate with an accuracy of 91.667%, showing that the recognition accuracy is not particularly good. The accuracy and recognition speed of accelerated intention recognition is directly impacted by the penalty parameter c and kernel function parameter g in the support vector machine model for accelerated intention recognition.

Table 1. Partial Sample Data.

Accelerator pedal opening	Accelerator pedal opening change rate	Acceleration intention
0.3103	0.2190	1
0.7148	0.1715	2
0.7760	0.7151	3
0.3247	0.0459	1
0.1218	0.6813	2
0.6431	0.9917	3

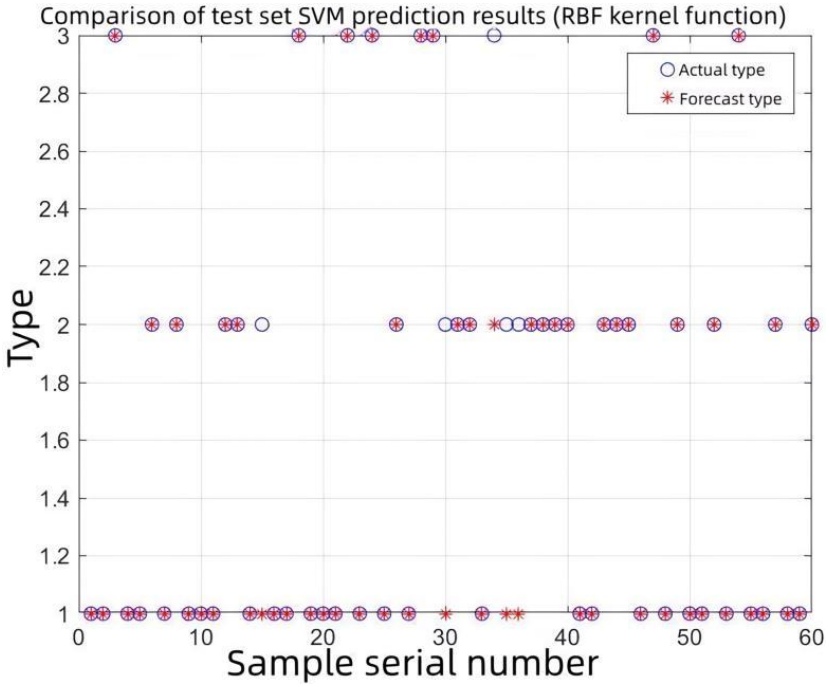

Figure 1. SVM Classification Resul.

2.1.2. Accelerating Intent Recognition Based on SSA Optimization of SVM Parameters

SSA is used to optimize the SVM parameters, with recognition accuracy as the fitness value, to increase the accuracy of the SVM model in identifying the acceleration intention of racing drivers and decrease the optimization time of the SVM model penalty parameter c and kernel function parameter g.

The steps for the Sparrow Search method (SSA), a new swarm intelligence optimization method that is primarily motivated by the predatory and anti-predatory behavior of sparrows, are as follows:

1) First, determine the inputs and outputs of the driving intention recognition model. Select the

accelerator pedal opening and the rate of change of the accelerator pedal opening as inputs to the recognition model, with the acceleration intention as the output value. According to the driver's intention to accelerate, it can be divided into three categories: slow acceleration, general acceleration, and rapid acceleration, represented by 1, 2, and 3, respectively. Establish training and testing sample values.

2) Then initialize the parameters of the sparrow search algorithm and support vector machine, including population size, maximum number of iterations, SVM parameters c, g.

3) Calculate the fitness values of all sparrows and determine the current optimal fitness value and corresponding sparrow individual positions.

4) Calculate the warning value and update the location of the discoverer based on the size of the warning value.

5) Update the position of the joiner based on the formula.

6) Update the warning sparrow position according to the formula.

7) Calculate the fitness value of sparrow individuals in the population after updating their positions, compare the updated fitness value with the previous optimal fitness value, and update the global optimal fitness value.

8) Determine whether the set iteration number condition is met. If not, repeat step 3). Otherwise, stop the iteration calculation and output the optimal parameters c and g. Input the test data set sample into the optimized SVM model and output the acceleration intent recognition result.

The flowchart of the SSA optimization SVM method is shown in Figure 2:

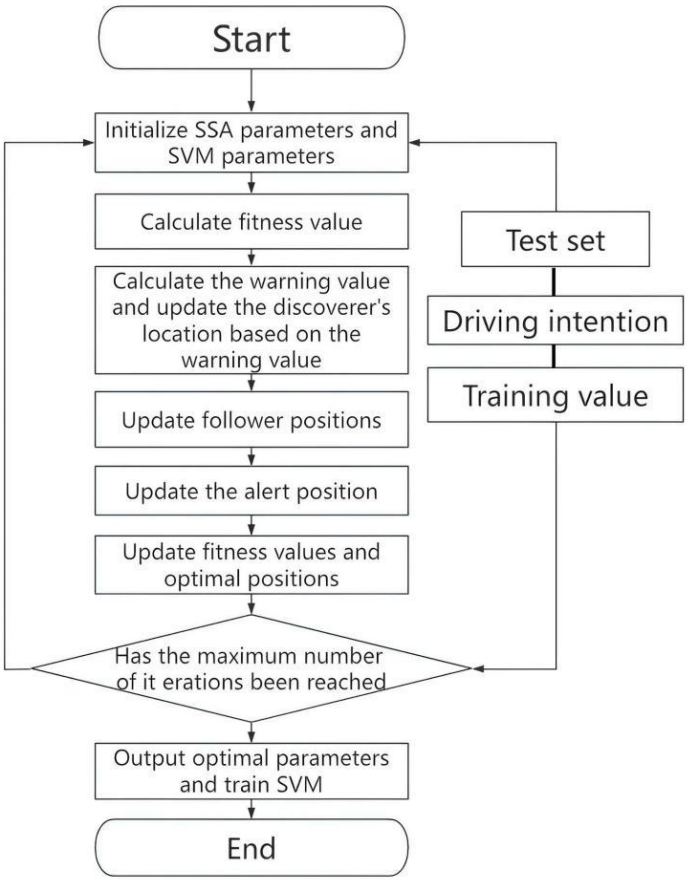

Figure 2. SSA optimization SVM flow chart.

In this article, we use Matlab software to train and test SSA-optimized SVM, normalize the sample data, set the optimization range of c and g to $[10^{-2}, 10^{-1}]$, and use the fitness function as the recognition accuracy to obtain the optimal parameters. After optimizing the sparrow search algorithm, the classification accuracy of the support vector machine reached 98.333%, and only one out of 60 test samples was misclassified. The classification results are shown in Figure 3.

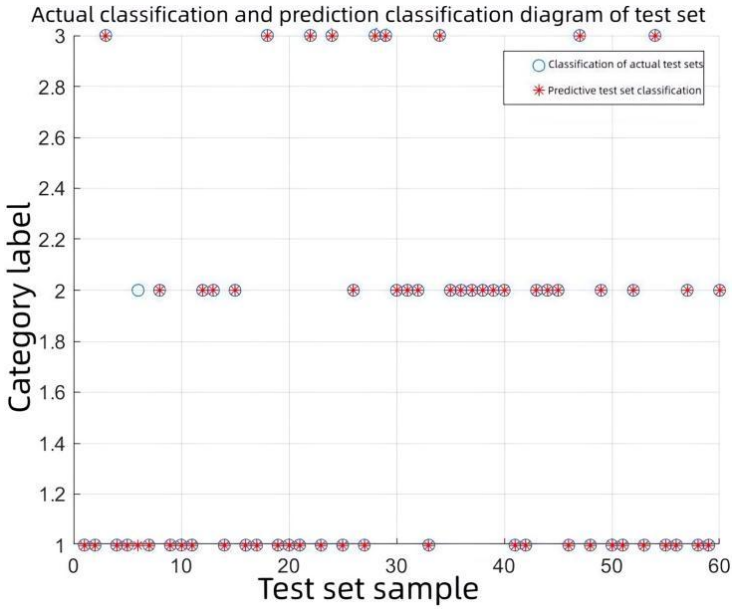

Figure 3. SSA-optimized SVM classification results.

Table 2 compares the outcomes of three SVM-accelerated intention recognition methods: SVM-accelerated intention recognition with initial parameters set; SVM-accelerated intention recognition with particle swarm optimization; and SVM-accelerated intention recognition with sparrow search algorithm optimization.

Table 2. Comparison of different optimization algorithms.

Arithmetic	Recognition accuracy	Value of c	Prime Time
SVM	91.6667%	1	-
PSO-SVM	96.6667%	9.6411	20.1727 s
SSA-SVM	98.3333%	7.8044	2.9137 s

Table 2 offers a comparative evaluation of three optimization algorithms: Support Vector Machine (SVM), Particle Swarm Optimization-based SVM (PSO-SVM), and Sparrow Search Algorithm-based SVM (SSA-SVM). This analysis focuses on three pivotal metrics: Recognition accuracy, parameter 'c' values, and optimization duration. While SVM demonstrates a recognition accuracy of 91.6667%, both PSO-SVM and SSA-SVM elevate this to 96.6667% and 98.3333%, respectively. As for 'c' values, the parameters stand at 1 for SVM, 9.6411 for PSO-SVM, and 7.8044 for SSA-SVM, highlighting distinct parameter tuning approaches among these algorithms. Regarding optimization time, PSO-SVM records the lengthiest span at 20.1727 seconds, whereas SSA-SVM curtails this to a mere 2.9137 seconds. In essence, while conventional SVMs might be quicker, they

lag in accuracy compared to their optimized counterparts. Both PSO-SVM and SSA-SVM manifest considerable accuracy improvements. Notably, SSA-SVM achieves this without compromising on speed, striking an impressive equilibrium between precision and efficiency. Hence, SVM models fine-tuned via the Sparrow Search Algorithm outperform those optimized by Particle Swarm Optimization, particularly in discerning a racing driver's acceleration intent.

2.2. Torque control strategy

The driving torque control strategy for a racing car is crafted to fulfill specific objectives. First, it aims to optimize the power performance of the vehicle, with the driving motor serving as its primary power source. This necessitates the motor possessing robust torque response characteristics while operating within the high-efficiency range. Second, it aims to ensure that the Formula One races can be completed within the energy consumption limits of the power battery, thereby satisfying mileage requirements. Presently, the prevalent driving torque control strategy is the linear torque control approach, known for its straightforward implementation and ability to fulfill fundamental driving needs. However, it frequently falls short of delivering adequate torque response, resulting in insufficient power to match the driver's driving intentions. To better address the acceleration needs of electric racing cars, we propose determining the motor's output torque based on the driver's driving intentions. To effectively meet the demand for acceleration in electric racing cars, this study suggests determining the motor's output torque by the driver's driving intentions. This is achieved through the utilization of a calculation method involving base torque and compensation torque. The base torque is established through a linear look-up table that considers the accelerator pedal opening and motor speed, while the compensation torque is derived from fuzzy torque calculations based on the positive and negative rates of change of the accelerator pedal opening.

2.2.1. Starting mode torque control

To guarantee the electric racing car's improved start acceleration performance and win the race, the drive motor's output torque in the start mode should satisfy the driver's requirement for the start acceleration torque. In this study, the maximum adhesion torque is used as the final starting torque. To reduce the starting impact, the basic torque is determined by the opening of the accelerator pedal, and the compensation torque is added to arrive at the final torque. At this point, the racing driver's pedal operation time has a buffering effect.

Starting torque control strategy: A base torque is determined from the accelerator pedal opening at the initial stage of starting, and then the difference of torque corresponding to the maximum adhesion force that can be provided by the ground is compensated until the racing car's operating mode is switched to the driving mode when the torque is calculated according to the driving mode. Figure 4 shows a schematic diagram of the starting torque of an electric racing car, where is the base torque determined by the accelerator pedal opening and is the torque corresponding to the maximum adhesion force.

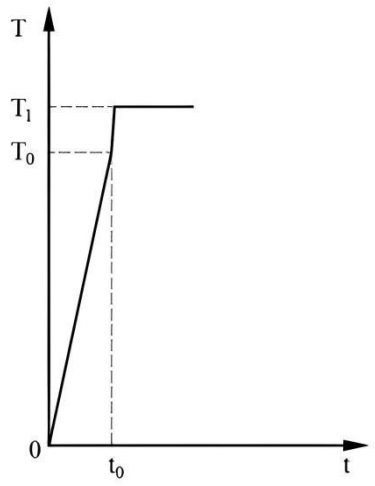

Figure 4. Schematic diagram of starting torque.

$$T_0 = k \cdot f(Accpdl) \tag{2}$$

Where T_0 represents the initial base torque, k is a proportionality factor, and *f*(Accpdl) is a function related to the accelerator pedal position. This function can be adjusted based on vehicle performance requirements and control strategies. In practical applications, the control system may employ a PID controller or other advanced control strategies to achieve precise control of the initial base torque. The specific relationship and parameter settings should be adjusted according to the specific design of the vehicle and the requirements of the control system.

$$T_{rq} = \frac{m(a+\delta a+\mu g)r}{i} \tag{3}$$

In Eq (3), m represents the mass of the car, a represents the acceleration of the car, and i represents the transmission ratio of the transmission system, μ is the rolling resistance coefficient, r is the wheel radius, g is the center of gravity acceleration, and d is the peak adhesion coefficient of the road surface. Specific parameter raw data for the vehicle can be found in Table 5 of Section 3.1, 'Modeling and Simulation Analysis'.

2.2.2. Driving mode torque control

The base torque plus compensation torque is used for torque control in driving mode, and the compensation torque is favorably and negatively compensated following the positive and negative rates of change of the pedal opening, respectively.

1) Basic torque design

In the drive torque control of an electric racing car, to enable the drive motor to operate efficiently, safely, and reliably, each rotational speed of the motor corresponds to maximum torque, and the actual torque of the motor is not the maximum torque at this moment, so to describe the mathematical relationship between the maximum torque of the motor and the actual torque, it is expressed through the introduction of a torque loading coefficient, L, which is the ratio of the motor's demanded torque to the motor's current rotational speed at which the motor's maximum torque is

correspondent to the current rotational speed of the motor, and the corresponding relationship of the accelerator pedal openness to the motor drive torque is transformed into the relationship with the torque loading coefficient, viz:

$$\begin{cases} T_{rq} = L \cdot T_{max}(n) \\ L = f(AccPdl) \end{cases} \tag{4}$$

In the Eq (4):T_{rq} is the demand torque, L is the motor torque load coefficient, with a range of [0,1], $T_{max}(n)$ is the motor peak torque at n speed, AccPdl is the accelerator pedal opening, $0 \leq AccPdl \leq 100\%$, and $AccPdl = 100\%$ is the accelerator pedal fully open.

According to the working characteristics and torque load curve of the driving motor, the torque in the constant torque and constant power regions is represented as follows:

$$T_{rq} = \begin{cases} L \cdot T_{max}(0 \leq n \leq n_0) \\ L \cdot \frac{9550 P_{max}}{n}(n_0 \leq n \leq n_{max}) \end{cases} \tag{5}$$

In the Eq (5):n_0 is the rated speed of the motor; P_{max} is the peak power of the motor; n is the current speed of the motor; n_{max} is the maximum speed of the motor.

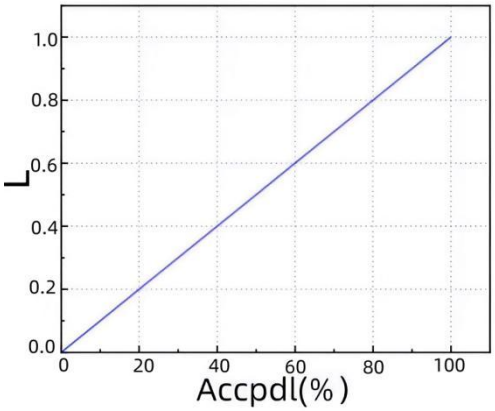

Figure 5. Linear Control Strategy.

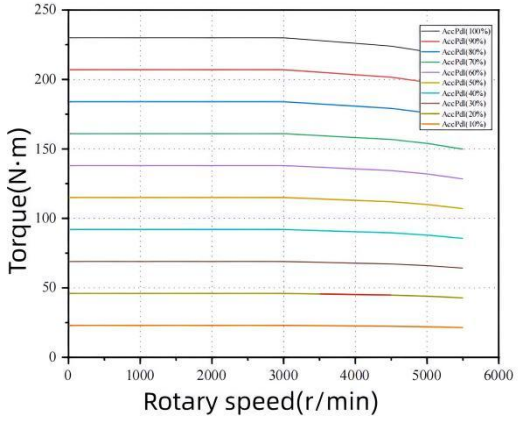

Figure 6. Linear mode motor torque map.

Under a linear control method, Figure 5 depicts the relationship curve between the opening of the accelerator pedal and the torque load coefficient. Figure 6 depicts the linear mode MAP diagram's related relationship between motor speed and associated torque.

2) Positive torque compensation design

During the acceleration of a racing car, the motor's torque response must be both rapid and smooth. Sudden variations in torque can result in vibrations and shocks during swift acceleration, causing vehicle instability and handling challenges, ultimately impacting the car's overall performance. To ensure handling stability and enhance overall safety, it is imperative to restrict torque compensation during acceleration. Determining a moderate maximum value for torque compensation helps mitigate the sensation of shock, contributing to a smoother acceleration experience.

$$j = \frac{da}{dt} = \frac{d^2v}{dt^2} \approx \frac{1}{m}\left(\frac{i\eta}{r} \cdot \frac{dT}{dt}\right) \tag{6}$$

In the Eq (6), j represents the impact, m represents the mass of the entire vehicle, r represents the tire radius, η represents the system transmission efficiency, i represents the transmission ratio, T represents the torque, and the above equation can be changed to:

$$\frac{dT}{dt} \approx \frac{mr}{i\eta} \cdot j \tag{7}$$

Usually, the German impact standard is used, $j \leq 10\mathrm{m/s}^3$, where the theoretical response time of the motor is calculated as 20ms, and the maximum acceleration torque compensation value can be calculated to be about $5\ \mathrm{N \cdot m}$.

Selecting the SSA optimized SVM model to identify the racing driver's acceleration intention and the current accelerator pedal opening as the input of the fuzzy controller, the motor acceleration compensation torque $\mathrm{T_c}$ as the output variable, and the membership function and fuzzy rules of the input and output variables are described as follows:

The range of accelerator pedal opening is [0,1], and its fuzzy set domain is [0,1]. The fuzzy subset is divided into 5 levels, namely {negative small, small, medium, large, positive large}, denoted as {NB, NS, ZO, PS, PB}; the acceleration intentions of three types of racing drivers identified by SSA optimized SVM models are represented by numbers 1, 2, and 3, respectively. The fuzzy set domain of acceleration intentions is [0.5,3.5], and is divided into three levels: {small, medium, and large}, denoted as {S, ZO, B}. The fuzzy set theory domain of motor acceleration torque compensation is set to [0,5] based on the calculated maximum compensation torque, divided into 5 levels, {negative small, small, medium, large, positive large}, denoted as {NB, NS, ZO, PS, PB}, respectively. Triangular and trapezoidal functions are selected as the membership functions of each variable, as shown in Figure 7, where Figure 7a is the membership function image of the accelerator pedal opening, Figure 7b is the membership function image of the acceleration intention, and Figure 7c is the membership function image of the motor compensation torque.

Establish fuzzy control rules. When a racing driver has a strong demand for torque and their objective is to accelerate quickly, this is reflected in the size of the pedal opening. To guarantee the race car's ability to accelerate, a higher compensatory torque needs to be offered. To achieve better economy, the compensatory torque should instead be decreased to accommodate the driving requirements of the race driver. Table 3 displays the rules for fuzzy inference.

The "Mamdani" fuzzy inference approach and the center of gravity method were utilized to resolve the ambiguity while designing a fuzzy controller in Matlab using the Fuzzy Logic Designer toolbox. Figure 7d depicts the surface of the fuzzy inference connection that was obtained. The fuzzy rule surface shows that the acceleration intention is stronger and the compensatory torque is bigger the wider the pedal opening.

Table 3. Fuzzy Reasoning Rules Table.

Acceleration intention	Accelerator pedal opening				
	NB	NS	ZO	PS	PB
S	NB	NB	NS	ZO	PS
ZO	NB	NS	ZO	PS	PB
B	NS	ZO	PS	PB	PB

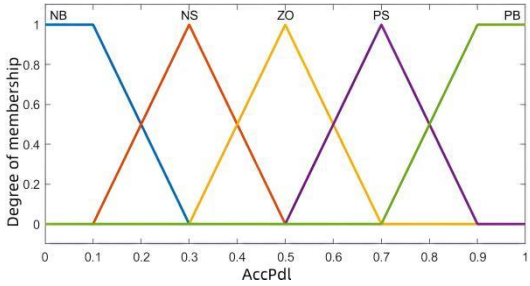

a) Accelerator pedal opening membership function.

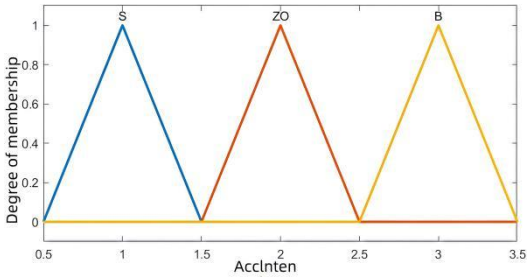

b) Accelerated Intent Membership Function.

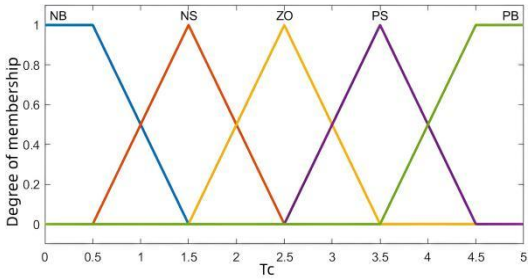

c) Motor torque compensation membership function.

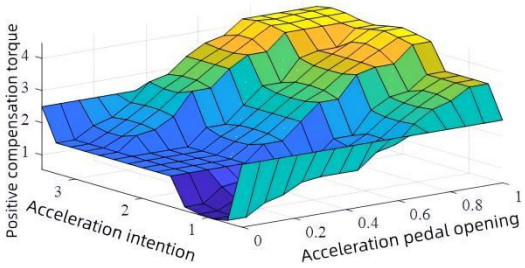

d) Fuzzy Rule Control Surface.

Figure 7. Positive torque fuzzy control.

The driving torque of a racing car in driving mode is the sum of the basic torque and compensation torque, which is:

$$T_{cmd} = T_{rq} + T_c \tag{8}$$

3）Negative torque compensation design

Considering the economy of the racing car, the driver compensates for negative torque when retracting the accelerator pedal. At this point, the driver has the intention to slow down and reduce the output of the driving torque while meeting the power requirements. Using a fuzzy control algorithm to compensate for negative torque, the input is the absolute value of the current vehicle speed and the change rate of the accelerator pedal opening, and the output is the negative torque compensation value. The maximum value of negative torque compensation based on the impact degree is 5N. The input range of vehicle speed v is defined as [0,130], which divides the fuzzy subset of vehicle speed into 5 levels, {negative small, small, medium, large, positive large}, denoted as {NS, S, ZO, B, NB}, respectively. The input range of the absolute value of the accelerator pedal change rate Acc Rate is defined as [0,4], and its fuzzy subset is evenly divided into 5 levels, {negative small, small, medium, large, positive large} denoted as {NS, S, ZO, B, NB}, respectively. The input range, fuzzy subset, and language value definition of negative torque compensation value are the same as those of positive torque compensation. The membership function of the input and output of negative torque compensation is shown in Figure 8, where Figure 8a is the membership function image of the absolute value of the accelerator pedal opening change rate, Figure 8b is the membership function image of the vehicle speed, and Figure 8c is the membership function image of negative torque compensation.

Create fuzzy control rules to compensate for negative torque. When the vehicle speed is high and the change rate of the accelerator pedal is large in absolute terms, it means that the driver intends to reduce the vehicle speed rapidly and does not require a lot of torque from the driving motor. Increase the negative torque compensation now. Conversely, it shows that the driver anticipates stable driving at a low speed when the absolute value of the change rate of the accelerator pedal is minimal and the vehicle speed is similarly small. Reduce negative torque compensation at this moment. Figure 8d displays the fuzzy surface diagram for negative torque compensation, and Table 4 displays the fuzzy inference table for this purpose.

Table 4. Negative torque compensation fuzzy inference table.

Speed of a motor vehicle	The absolute value of accelerator pedal opening change rate				
	NS	S	ZO	B	NB
NS	NS	NS	S	S	ZO
S	NS	S	S	ZO	ZO
ZO	S	S	ZO	B	B
B	S	ZO	B	B	NB
NB	ZO	B	B	NB	NB

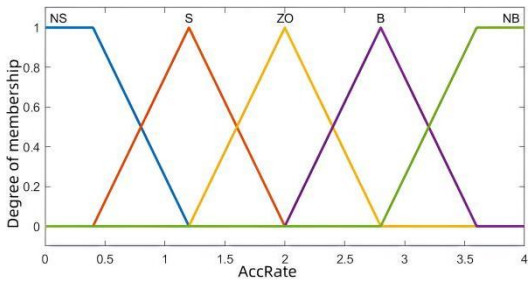

a) Membership Function of Absolute Value of Pedal Opening Change Rate.

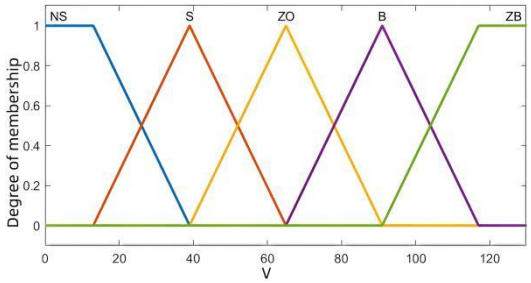

b) Vehicle speed membership function.

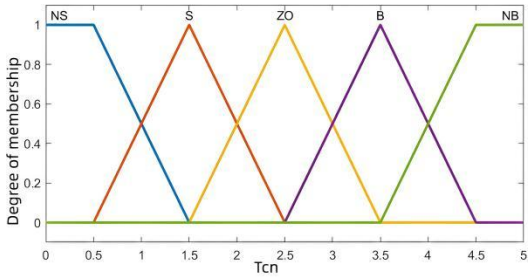

c) Negative torque compensation membership function.

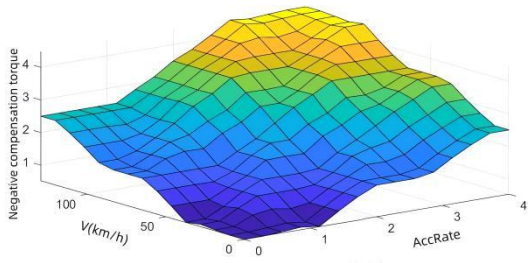

d) Negative torque compensation fuzzy surface.

Figure 8. Negative torque fuzzy control.

3. Methods and experiments

3.1. Modeling and simulation analysis

Matlab/Simulink is used to build the acceleration intention recognition-based torque control strategy for electric racing cars, and the Cruise Interface CMC is used for collaborative simulation with AVL Cruise. To compare the durability of the race project with the 75m linear acceleration for simulation, the simulation results of the drive control method can be shown in Simulink's post-processing module. The rules of the competition have clear provisions for the wheelbase, wheelbase, position of the pneumatic kit the dimensions of the key stress positions of the frame of the electric racing car, etc. As shown in Table 5 for the electric racing car of this study, the basic parameters of the car, and the performance design objectives of the racing car, as well as some of the major parameters of the drive motor, which are used to carry out the simulation test on the software.

Table 5. Basic vehicle parameters.

Technical Parameter	Numerical value	Performance goals	Numerical value
Vehicle mass (kg)	280 (including driver 345)	Maximum speed (km/h)	125
Tire radius (mm)	226	Acceleration time from 0 to 75m (s)	4.5
Windward area (m^2)	0.9	Maximum acceleration (m/s^2)	10
Air resistance coefficient	0.35	Range (km)	22
Rolling Resistance Coefficient	0.015	**Main Parameters of Motor**	**Numerical value**
Center of gravity height (m)	300	Rated power/peak power (kW)	28-42/100
Track width front/rear (mm)	1230/1180	Rated torque/peak torque (Nm)	120/230
Transmission efficiency	90%	Maximum speed (RPM)	5500

Figure 9 depicts the speed curve under durability conditions, and it can be seen that the current speed closely resembles the desired speed. Figure 10 displays the results of our recognition of the acceleration intentions of racing drivers under durability conditions. Numbers 1 and 2 denote slow acceleration, general acceleration, and emergency acceleration, respectively. Number 3 denotes emergency acceleration. Figure 11 depicts the fuzzy control positive torque compensation utilized to increase the race car's power output when the accelerator pedal opening change rate is positive. Figure 12 illustrates the negative torque compensation under fuzzy control when the change rate of the accelerator pedal opening is negative. Since the racer is slowing down, boosting negative torque adjustment can somewhat cut down on power consumption.

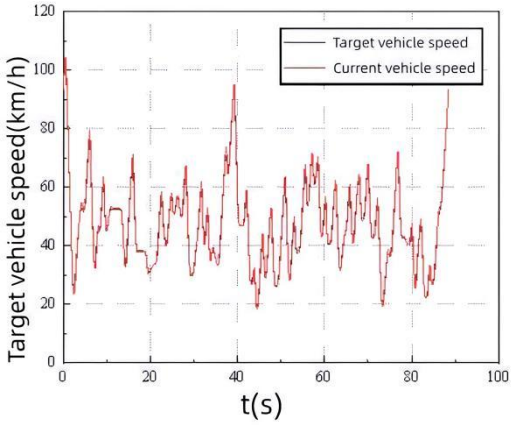

Figure 9. Durability Working Condition Speed Curve.

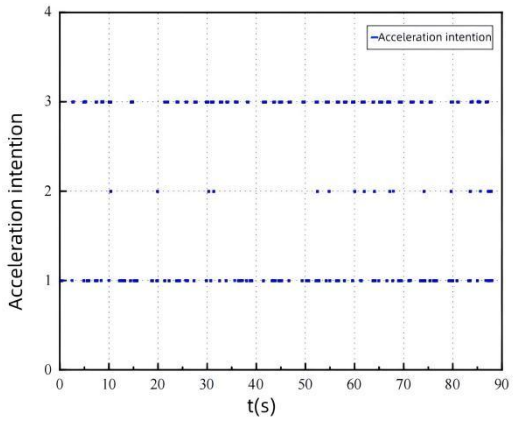

Figure 10. Accelerated Intent Recognition.

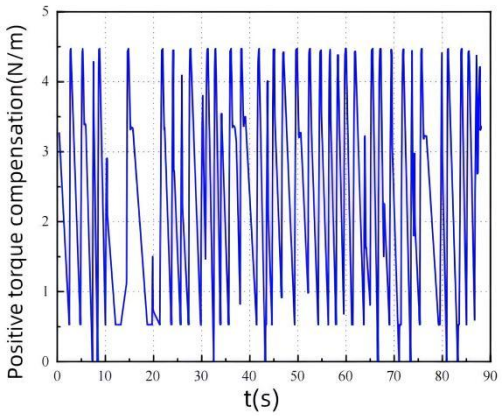

Figure 11. Positive torque compensation.

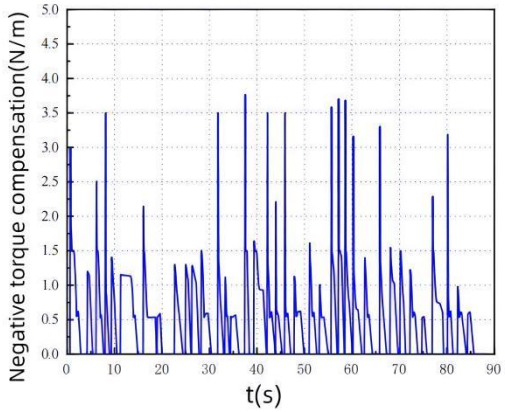

Figure 12. Negative torque compensation.

To simulate the 75 m linear acceleration project of a race automobile, we create a full load acceleration task in the Cruise software. The simulation results are displayed in Figure 13. The 75m linear acceleration takes 4.36 seconds without the control method, and 4.13 seconds with the control strategy, according to the study of simulation findings. This demonstrates that the time required is reduced by 0.23 seconds, enhancing the race car's power output. Furthermore, the speed of the car is much higher than when no control plan is introduced because starting torque compensation has been provided.

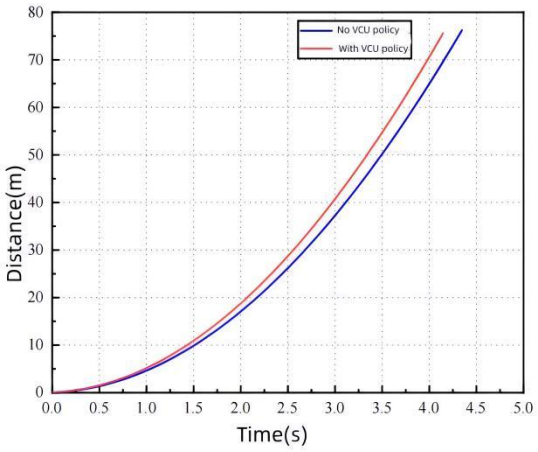

Figure 13. Comparison of Racing Distance.

Table 6 shows the comparison of policy state information for FSEC electric racing car 75m acceleration simulation with and without VCU (Vehicle Control Unit) policy. The table lists the gear position, time, speed (V), and T time at different distances. In the absence of VCU policy, the time taken increases from 0.42 seconds to 4.36 seconds and the speed increases from 14.06 km/h to 119.47 km/h as the distance increases from 1 to 75 meters. With the VCU policy, the time increased from 0.38 to 4.13 seconds and the speed increased from 14.84 to 123.96 km/h. For each distance point, the speeds were slightly higher with the VCU policy than without it. This means that the VCU policy may have had a positive effect on vehicle control, increasing speed without significantly increasing time. The gear position at each distance point remained in 1st gear, suggesting that the vehicle may have remained in the same gear throughout the 75-meter test distance. Overall, the VCU policy appears to have had a positive impact on vehicle performance, particularly in terms of increasing speed.

Table 6. Comparison of Strategy Status Information for 75m with or without VCU.

		No VCU policy		With VCU policy	
Distance（m）	Gear position（-）	Time（s）	V（km/h）	T（s）	V（km/h）
1	1	0.42	14.06	**0.38**	**14.84**
2	1	0.64	19.93	**0.58**	**21.01**
3	1	0.80	24.43	**0.74**	**25.73**
20	1	2.20	62.90	**2.07**	**66.14**
40	1	3.15	88.59	**2.97**	**92.92**
60	1	3.88	107.75	**3.67**	**112.16**
75	1	4.36	119.47	**4.13**	**123.96**

3.2. Hardware in the loop test

We conduct hardware-in-the-loop testing analysis on the durability and 75m straight-line operating conditions of FSEC electric racing cars. It is necessary to compile the entire vehicle model

in AVL Cruise into NI Veriland's executable dynamic link library (DLL) files based on the task folder.

The durability map of the FSEC electric racing vehicles is depicted in Figure 14, and it demonstrates that the hardware in the loop test speed can closely approach the goal speed.

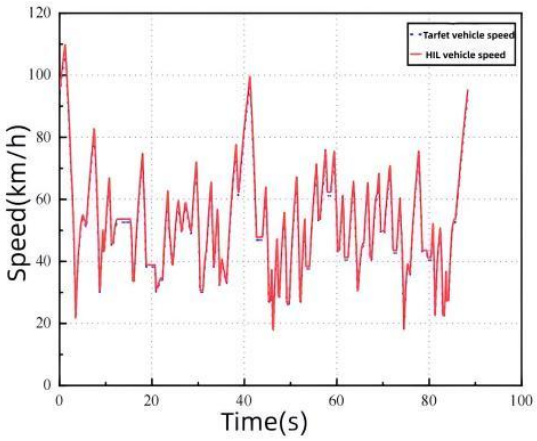

Figure 14. Durability Test Track Speed.

The endurance single-lap driving distance of NI hardware in the loop test is 1163.38m, as shown in Figure 15, which is a comparison between the endurance race track simulation and NI hardware in the loop test. The endurance single lap driving distance under the joint simulation of AVL Cruise and Simulink is 1164.65m. Figure 16 shows the schematic diagram of the distance error between the joint simulation and NI hardware in the loop testing. Analysis shows that the maximum error is 0.504%, and the average error is 0.109%. From this, it can be seen that the error between the simulation results and the hardware in the loop results is within 1%, and the two are the same.

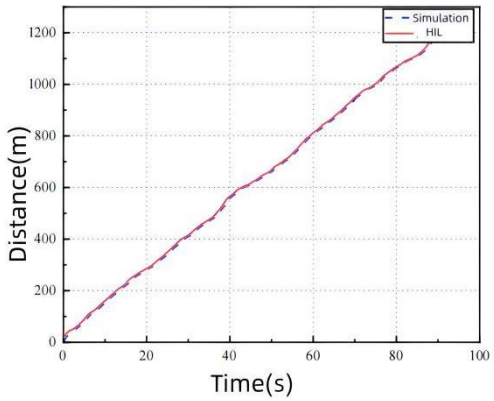

Figure 15. Comparison of distance between simulation and HIL testing.

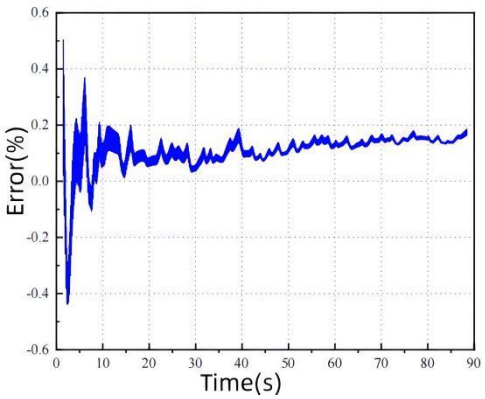

Figure 16. Simulation and HIL Testing Errors.

Table 7. Comparison of 75m Linear Acceleration Simulation and Hardware in the Loop Test Results.

	Simulation	HIL
Time（s）	V（km/h）	V（km/h）
0.38	14.84	14.73
0.98	33.20	33.01
1.95	62.78	62.27
2.56	80.79	80.12
3.34	103.17	102.96
4.07	122.48	121.34

Table 7 shows the comparison between the 75 m linear acceleration simulation and the Hardware-in-the-Loop (HIL) test results. The table lists the vehicle speeds at different time points, divided into simulated and HIL values. At 0.38 seconds, the simulated speed is 14.84 km/h, while the HIL speed is slightly lower at 14.73 km/h. Both sets of data show an increase in speed over time, but the HIL readings are slightly lower than the simulated values at each time point. At 0.98 seconds, the simulated value was 33.20 km/h and the HIL value was 33.01 km/h; at 1.95 seconds, the simulated value was 62.78 km/h and the HIL value was 62.27 km/h; at 2.56 seconds, the simulated value was 80.79 km/h and the HIL value was 80.12 km/h; at 3.34 seconds, the simulated value was 103.17 km/h and the HIL value is 102.96 km/h; finally, at 4.07 s, the simulated value reaches 122.48 km/h and the HIL value is 121.34 km/h. Overall, the results of the HIL test are very close to the simulation results, indicating that the simulation model can predict the performance of the actual hardware with a high degree of accuracy.

4. Conclusion

Through the joint simulation of Matlab/Simulink and AVL Cruise software as well as the NI hardware-in-the-loop test, the hardware-in-the-loop test results of the FSEC electric racing car in the endurance condition and the 75m straight-line acceleration condition are the same as the simulation results, which verifies the effectiveness of the torque control strategy based on the driver's intention recognition and enhances the dynamics of the racing car. The support vector machine (SVM) is used to identify the three acceleration intentions of the driver by using the accelerator pedal opening and its rate of change as the feature parameters. Moreover, the penalty parameter c and kernel function parameter g in the SVM are optimized by the sparrow search algorithm, which can significantly shorten the optimization time and increase the identification accuracy. The racing car is divided into two modes: Start and drive, both of which use the base torque and compensation torque calculation. The torque compensation for the starting mode is determined by the difference between the base torque and the maximum adhesion torque, while the torque compensation for the driving mode is based on the positive or negative change rate of the accelerator pedal opening using a fuzzy control method. The racing car can follow the target speed better, the driving torque is compensated according to the control strategy during driving, the matching of power system parameters meets the requirements, and the starting dynamics are also improved.

We propose a torque control strategy based on driving intention recognition, which achieves

certain results of the intended design. However, there are some limitations due to the experimental conditions. For example, we focus on acceleration intention recognition, while an in-depth study of the driver's turning and braking intentions during racing car driving has not yet been fully developed, and thus a more comprehensive drive control strategy is yet to be developed. Future work should include a real-car track test after the completion of the racing car to further validate the effectiveness and reasonableness of the drive control strategy and to improve and promote the research and application in this field.

Use of AI tools declaration

The authors declare they have not used Artificial Intelligence (AI) tools in the creation of this article.

Conflict of interest

The authors declare that there are no conflicts of interest.

References

1. W. Li, G. Zhao, Y. Zhu, X. Lin, Y. Zhang, Research on compound braking control strategy of extended-range electric vehicle based on driving intention recognition, *Comput. Intell. Neurosci.*, **2022** (2022), 8382873. https://doi.org/10.1155/2022/8382873
2. X. Zhang, B. Zu, J. Zhou, S. Liang, Research on torque control method of hybrid electric vehicle based on driving intention recognition, in *2021 5th CAA International Conference on Vehicular Control and Intelligence (CVCI)*, (2021), 1–6. https://doi.org/10.1109/CVCI54083.2021.9661243
3. Y. Guo, H. Zhang, C. Wang, Q. Sun, W. Li, Driver lane change intention recognition in the connected environment, *Phys. A Statist. Mechan. Appl.*, **575** (2021), 126057. https://doi.org/10.1016/j.physa.2021.126057
4. S. Wang, X. Zhao, Q. Yu, Vehicle stability control strategy based on recognition of driver turning intention for dual-motor drive electric vehicle, *Math. Problems Eng.*, **2020** (2020), 3143620. https://doi.org/10.1155/2020/3143620
5. Y. Liu, P. Zhao, D. Qin, G. Li, Y. Zhang, Driving intention identification based on long short-term memory and a case study in shifting strategy optimization, *IEEE Access*, **7** (2019), 128593–128605. https://doi.org/10.1109/ACCESS.2019.2940114
6. L. Tang, H. Wang, W. Zhang, Z. Mei, L. Li, Driver lane change intention recognition of intelligent vehicle based on long short-term memory network, *IEEE Access*, **8** (2020), 136898–136905. https://doi.org/10.1109/ACCESS.2020.3011550
7. Q. Shangguan, T. Fu, J. Wang, S. Fang, L. Fu, A proactive lane-changing risk prediction framework considering driving intention recognition and different lane-changing patterns, *Accident Anal. Prevent.*, **164** (2022),106500. https://doi.org/10.1016/j.aap.2021.106500
8. K. Gao, P. Luo, J. Xie, B. Chen, Y. Wu, R. H. Du, Energy management of plug-in hybrid electric vehicles based on speed prediction fused driving intention and LIDAR, *Energy*, **284** (2023), 128535. https://doi.org/10.1016/j.energy.2023.128535
9. J. Ju, L. Bi, A. G. Feleke, Noninvasive neural signal-based detection of soft and emergency

braking intentions of drivers, *Biomed. Signal Process. Control*, **72** (2022), 103330. https://doi.org/10.1016/j.bspc.2021.103330
10. T. Han, J. Jing, Ü. Özgüner, Driving intention recognition and lane change prediction on the highway, in *2019 IEEE Intelligent Vehicles Symposium (IV)*, (2019), 957–962. https://doi.org/10.1109/IVS.2019.8813987
11. Q. Shangguan, T. Fu, J. Wang, S. Fang, L. Fu, A proactive lane-changing risk prediction framework considering driving intention recognition and different lane-changing patterns, *Accident Anal. Prevent.*, **164** (2022), 106500. https://doi.org/10.1016/j.aap.2021.106500
12. R. Yuan, M. Abdel-Aty, X. Gu, O. Zheng, Q. Xiang, A unified modeling framework for lane change intention recognition and vehicle status prediction, *Phys. A Statist. Mechan. Appl.*, **632** (2023), 129332. https://doi.org/10.1016/j.physa.2023.129332
13. C. Zong, C. Wang, D. Yang, H. Yang, Driving intention identification and maneuvering behavior prediction of drivers on cornering, in *2009 International Conference on Mechatronics and Automation,* (2009), 4055–4060. https://doi.org/10.1109/ICMA.2009.5246638
14. F. Zhao, B. Xie, Y. Tian, Multi-parameter driver intention recognition based on neural network, in *2020 4th CAA International Conference on Vehicular Control and Intelligence (CVCI)*, (2020), 130–135. https://doi.org/10.1109/CVCI51460.2020.9338444
15. S. Liu, K. Zheng, L. Zhao, P. Fan, A driving intention prediction method based on hidden Markov model for autonomous driving, *Computer Commun.,* **157** (2020), 143–149. https://doi.org/10.1016/j.comcom.2020.04.021
16. H. Ma, Y. Wang, R. Xiong, S. Kodagoda, L. Tang, DeepGoal: Learning to drive with driving intention from human control demonstration, *Robotics Autonom. Syst.*, **127** (2020), 103477. https://doi.org/10.1016/j.robot.2020.103477
17. Y. Li, H. Hong, D. Luigi, Y. Ye, Research on driving control strategy of an electric racing car based on pattern recognition, in *Proceedings of China SAE Congress 2021: Selected Papers*, **818** (2023), 578–591. https://doi.org/10.1007/978-981-19-3842-9_46
18. J. Wang, Y. Cai, L. Chen, D. Shi, R. Wang, Z. Zhu, Review on multi-power sources dynamic coordinated control of hybrid electric vehicle during driving mode transition process, *Int. J. Energy Res.*, **44** (2020), 6128–6148. https://doi.org/10.1002/er.5264
19. T. Pan, H. Zang, Anti-jerking and traction torque compensation strategy for $P3^+$ hybrid electric vehicle during power upshift, *Proceed. Instit. Mechan. Eng. Part D J. Autom. Eng.,* **237** (2023), 587–606. https://doi.org/10.1177/09544070221085384
20. J. Hu, C. Sun, J. Xiao, J. Li, A torque compensation strategy in two-speed automated mechanical transmission shift process for pure electric vehicles, *Adv. Mechan. Eng.*, **7** (2015), 441–444. https://doi.org/10.1177/1687814015616915
21. S. Xu, L. Wei, X. Zhang, Z. Bai, Y. Jiao, Research on Multi-Mode Drive Optimization Control Strategy of Four-Wheel-Drive Electric Vehicles with Multiple Motors, *Sustainability*, **14** (2022), 7378. https://doi.org/10.3390/su14127378
22. S. Kitayama, M. Saikyo, Y. Nishio, K. Tsutsumi, Torque control strategy and optimization for fuel consumption and emission reduction in parallel hybrid electric vehicles, *Struct. Multidisc. Optim.*, **52** (2015), 595–611. https://doi.org/10.1007/s00158-015-1254-8
23. F. Zhang, X. Hu, R. Langari, L. Wang, Y. Cui, H. Pang, Adaptive energy management in automated hybrid electric vehicles with flexible torque request, *Energy*, **214** (2020), 118873. https://doi.org/10.1016/j.energy.2020.118873

24. S. Li, B. Sarlioglu, S. Jurkovic, N. R. Patel, P. Savagian, Comparative analysis of torque compensation control algorithms of interior permanent magnet machines for automotive applications considering the effects of temperature variation, *IEEE Trans. Transp. Electrif.*, **3** (2017), 668–681. https://doi.org/10.1109/TTE.2017.2684080
25. Z. Yu, Y. Hou, B. Leng, L. Xiong, Y. Li, Disturbance compensation torque coordinated control of four in-wheel motor independent-drive electric vehicles, *IEEE Access*, **8** (2022), 119758–119767. https://doi.org/10.1109/ACCESS.2020.3005943.
26. H. Wei, N. Zhang, J. Liang, Q. Ai, W. Zhao, T. Huang, et al., Deep reinforcement learning based direct torque control strategy for distributed drive electric vehicles considering active safety and energy saving performance, *Energy*, **238** (2022), 121725. https://doi.org/10.1016/j.energy.2021.121725
27. H. Wei, Q. A, W. Zhao, Y. Zhang, Modelling and experimental validation of an EV torque distribution strategy towards active safety and energy efficiency, *Energy*, 2**39** (2022), 121953. https://doi.org/10.1016/j.energy.2021.121953
28. X. Hu, P. Wang, Y. Hu, H. Chen, A stability-guaranteed and energy-conserving torque distribution strategy for electric vehicles under extreme conditions, *Appl. Energy*, **259** (2020), 114162. https://doi.org/10.1016/j.apenergy.2019.114162
29. J. Hu, J. Li, Z. Hu, B. Zhang, L. F. Xu, M. G. Ouyang, Energy-efficient torque-allocation strategy for a 6×6 vehicle using electric wheels, *eTransportation*, **10** (2021), 100136. https://doi.org/10.1016/j.etran.2021.100136
30. J. Wang, S. Gao, K. Wang, Y. Wang, Q. Wang, Wheel torque distribution optimization of four-wheel independent-drive, *Control Eng. Pract.*, **110** (2021), https://doi.org/10.1016/j.conengprac.2021.104779
31. X. Zhang, D. Göhlich, J. Li, Energy-efficient toque allocation design of traction and regenerative braking for distributed drive electric vehicles, *IEEE Transact. Vehic. Technol.*, **67** (2018), 285–295. https://doi.org/10.1109/TVT.2017.2731525
32. Q. Han, L. Zhu, J. Wang, D. Chen, Hopf-curve-based torque distribution strategy for avoiding limit cycle vibration in hybrid braking system model, *Int. J. Non-Linear Mechan.*, **154** (2023), 104440. https://doi.org/10.1016/j.ijnonlinmec.2023.104440
33. Y. Jiang, H. Meng, G. Chen, C. Yang, X. Xu, L. Zhang, Differential-steering based path tracking control and energy-saving torque distribution strategy of 6WID unmanned ground vehicle, *Energy*, **254** (2022), 124209. https://doi.org/10.1016/j.energy.2022.124209
34. Z. Zhang, T. Zhang, J. Hong, H. Zhang, J. Yang, Entropy-based torque control strategy of Mechanical–Electric–Hydraulic Power Coupling Vehicles, *Control Eng. Pract.*, **133** (2023), 105437. https://doi.org/10.1016/j.conengprac.2023.105437
35. C. Geng, B. Jin, X. Zhang, Research on torque control strategy for electric vehicle with in-wheel motor, *IFAC-PapersOnLine*, **51** (2018), 71–74. https://doi.org/10.1016/j.ifacol.2018.10.014
36. A. I. M. Almadi, R. E. Al Mamlook, Y. Almarhabi, I. Ullah, A. Jamal, N.Bandara, A fuzzy-logic approach based on driver decision-making behavior modeling and simulation, *Sustainability*, **14** (2022), 8874. https://doi.org/10.3390/su14148874
37. J. Heine, M. Sylla, I. Langer, T. Schramm, B. Abendroth, R. Bruder, Algorithm for driver intention detection with fuzzy logic and edit distance, in *2015 IEEE 18th International Conference on Intell. Trans. Syst.*, (2015), 1022–1027. https://doi.org/10.1109/ITSC.2015.170
38. W. Qi, Fuzzy control strategy of pure electric vehicle based on driving intention recognition, *J.*

Intell. Fuzzy Syst. Appl. Eng. Technol., **39** (2020), 5131–5139. https://doi.org/10.3233/JIFS-179998

39. F. Liu, A PMSM fuzzy logic regenerative braking control strategy for electric vehicles, *J. Intell. Fuzzy Syst*., **41** (2021), 4873–4881.https://doi.org/10.3233/JIFS-189972
40. S. Wang, X. Huang, J. M. López. X. Xu. P. Dong, Fuzzy adaptive-equivalent consumption minimization strategy for a parallel hybrid electric vehicle, *IEEE Access*, **7** (2019), 133290–133303. https://doi.org/10.1109/ACCESS.2019.2941399
41. K. Kakouche, T. Rekioua, S. Mezani, A. Oubelaid, D. Rekioua, V. Blazek, et al., Model predictive direct torque control and fuzzy logic energy management for multi power source electric vehicles, *Sensors*, **22** (2022), 5669. https://doi.org/10.3390/s22155669

AIMS Press